AD

Technical Report CCDCAC-BLTR-20002

MHD Electrolyte Flow Driven by a Sinusoidal Electric Field in an Inter-electrode Gap within a Constant Magnetic Field

Curtis Bradley[1]
Johnson Samuel[2]

[1]U.S. Army Combat Capabilities
Development Command Armaments Center
Benét Laboratories
Watervliet, NY 12189

[2]Department of Mechanical Aerospace and Nuclear Engineering
Rensselaer Polytechnic Institute
Troy, NY 12180

October 11, 2019

(THIS PAGE INTENTIONALLY LEFT BLANK)

The views, opinions, and/or findings contained in this report are those of the author(s) and should not be construed as an official Department of the Army position, policy, or decision, unless so designated by other documentation.

The citation in this report of the names of commercial firms or commercially available products or services does not constitute official endorsement by or approval of the U.S. Government.

Destroy this report when no longer needed by any method that will prevent disclosure of its contents or reconstruction of the document. Do not return to the originator.

REPORT DOCUMENTATION PAGE

Form Approved
OMB No. 0704-0188

1. REPORT DATE *(DD-MM-YYYY)*	2. REPORT TYPE	3. DATES COVERED *(From - To)*
11/10/2019	Technical Report	

4. TITLE AND SUBTITLE
MHD Electrolyte Flow Driven by a Sinusoidal Electric Field in an Inter-electrode Gap within a Constant Magnetic Field

5a. CONTRACT NUMBER

5b. GRANT NUMBER

5c. PROGRAM ELEMENT NUMBER

6. AUTHOR(S)
Curtis Bradley
Johnson Samuel

5d. PROJECT NUMBER

5e. TASK NUMBER

5f. WORK UNIT NUMBER

7. PERFORMING ORGANIZATION NAME(S) AND ADDRESS(ES)
U.S. Army Combat Capabilities Development Command
Armaments Center, Benét Laboratories Directorate
1 Buffington Street
Watervliet, NY 12189

8. PERFORMING ORGANIZATION REPORT NUMBER
CCDCAC-BLTR-20002

9. SPONSORING/MONITORING AGENCY NAME(S) AND ADDRESS(ES)

10. SPONSOR/MONITOR'S ACRONYM(S)

11. SPONSOR/MONITOR'S REPORT NUMBER(S)

12. DISTRIBUTION/AVAILABILITY STATEMENT
DISTRIBUTION STATEMENT A. Approved for public release; distribution is unlimited.

13. SUPPLEMENTARY NOTES

14. ABSTRACT
Pulsed electrochemical machining is a necessary extension to traditional ECM for small geometries and some high-performance materials like super alloys. Electrical current density is one of the limiting factors. The electrolyte flow in the inter-electrode gap can be assisted using a magnetic field to allow higher currents, but this creates a complex magnetohydrodynamic flow. This paper presents an experimental and computational study of electrolyte flow velocity driven by a sinusoidal electric field in an inter-electrode gap (IEG) within a constant magnetic field. The electrochemical impedance spectroscopy (EIS) experiments used a 7075 aluminum anode in an NaNO3 electrolyte that showed the effects of magnetic

15. SUBJECT TERMS
Pulsed electrochemical machining, ECM, super alloys, electrical current density, electrolyte flow, inter-electrode gap, IEG, magnetic field, high currents, magnetohydrodynamic flow, inusoidal electric field, electrochemical impedance spectroscopy, EIS, 7075 aluminum anode, NaNO3 electrolyte, electrochemical cell

16. SECURITY CLASSIFICATION OF:			17. LIMITATION OF ABSTRACT	18. NUMBER OF PAGES	19a. NAME OF RESPONSIBLE PERSON
a. REPORT	b. ABSTRACT	c. THIS PAGE			Curtis Bradley
					19b. TELEPHONE NUMBER *(Include area code)*
A	SAR	SAR	SAR	11	518-266-4858

INSTRUCTIONS FOR COMPLETING SF 298

1. REPORT DATE. Full publication date, including day, month, if available. Must cite at least the year and be Year 2000 compliant, e.g. 30-06-1998; xx-06-1998; xx-xx-1998.

2. REPORT TYPE. State the type of report, such as final, technical, interim, memorandum, master's thesis, progress, quarterly, research, special, group study, etc.

3. DATE COVERED. Indicate the time during which the work was performed and the report was written, e.g., Jun 1997 - Jun 1998; 1-10 Jun 1996; May - Nov 1998; Nov 1998.

4. TITLE. Enter title and subtitle with volume number and part number, if applicable. On classified documents, enter the title classification in parentheses.

5a. CONTRACT NUMBER. Enter all contract numbers as they appear in the report, e.g. F33315-86-C-5169.

5b. GRANT NUMBER. Enter all grant numbers as they appear in the report. e.g. AFOSR-82-1234.

5c. PROGRAM ELEMENT NUMBER. Enter all program element numbers as they appear in the report, e.g. 61101A.

5e. TASK NUMBER. Enter all task numbers as they appear in the report, e.g. 05; RF0330201; T4112.

5f. WORK UNIT NUMBER. Enter all work unit numbers as they appear in the report, e.g. 001; AFAPL30480105.

6. AUTHOR(S). Enter name(s) of person(s) responsible for writing the report, performing the research, or credited with the content of the report. The form of entry is the last name, first name, middle initial, and additional qualifiers separated by commas, e.g. Smith, Richard, J, Jr.

7. PERFORMING ORGANIZATION NAME(S) AND ADDRESS(ES). Self-explanatory.

8. PERFORMING ORGANIZATION REPORT NUMBER. Enter all unique alphanumeric report numbers assigned by the performing organization, e.g. BRL-1234; AFWL-TR-85-4017-Vol-21-PT-2.

9. SPONSORING/MONITORING AGENCY NAME(S) AND ADDRESS(ES). Enter the name and address of the organization(s) financially responsible for and monitoring the work.

10. SPONSOR/MONITOR'S ACRONYM(S). Enter, if available, e.g. BRL, ARDEC, NADC.

11. SPONSOR/MONITOR'S REPORT NUMBER(S). Enter report number as assigned by the sponsoring/ monitoring agency, if available, e.g. BRL-TR-829; -215.

12. DISTRIBUTION/AVAILABILITY STATEMENT. Use agency-mandated availability statements to indicate the public availability or distribution limitations of the report. If additional limitations/ restrictions or special markings are indicated, follow agency authorization procedures, e.g. RD/FRD, PROPIN, ITAR, etc. Include copyright information.

13. SUPPLEMENTARY NOTES. Enter information not included elsewhere such as: prepared in cooperation with; translation of; report supersedes; old edition number, etc.

14. ABSTRACT. A brief (approximately 200 words) factual summary of the most significant information.

15. SUBJECT TERMS. Key words or phrases identifying major concepts in the report.

16. SECURITY CLASSIFICATION. Enter security classification in accordance with security classification regulations, e.g. U, C, S, etc. If this form contains classified information, stamp classification level on the top and bottom of this page.

17. LIMITATION OF ABSTRACT. This block must be completed to assign a distribution limitation to the abstract. Enter UU (Unclassified Unlimited) or SAR (Same as Report). An entry in this block is necessary if the abstract is to be limited.

ABSTRACT

Pulsed electrochemical machining is a necessary extension to traditional ECM for small geometries and some high-performance materials like super alloys. Electrical current density is one of the limiting factors. The electrolyte flow in the inter-electrode gap can be assisted using a magnetic field to allow higher currents, but this creates a complex magnetohydrodynamic flow. This paper presents an experimental and computational study of electrolyte flow velocity driven by a sinusoidal electric field in an inter-electrode gap (IEG) within a constant magnetic field. The electrochemical impedance spectroscopy (EIS) experiments used a 7075 aluminum anode in an $NaNO_3$ electrolyte that showed the effects of magnetic field intensity and input voltage frequency on the current within the electrochemical cell. Computational analysis of the electrochemical cell showed the relation between the electromagnetic inputs and flowvelocity. By incorporating the experimental results into another computational analysis, the final simulation shows potential optimal operating conditions for magnetically assisted pulsed ECM.

Table of Contents

Abstract iv
Table of Contents v
List of Figures vi
List of Tables vi
1. Introduction 1
2. Theory 2
3. Experimental Design 3
4. Numerical Model 5
5. Results and Discussion 6
5.1 EIS Conductivity 6
5.2 MHD Simulation 7
5.3 EIS Driven MHD Simulation 8
6. Conclusion 9
Acknowledgments 9
References 9

List of Figures

Figure 3.1, Model of Experimental Flow Cell 4

Figure 3.2, Map of magnetic field flux density within the IEG with the inner cylinder representing the tool IEG and outer cylinder the workpiece 5

Figure 4.1, Simulation showing vectors for magnetic field, electric field, Lorentz force, and resulting electrolyteflow 6

Figure 5.1, ESI conductivity as a function of frequency and magnetic field flux density 7

Figure 5.2, Electrolyte velocity magnitude average over the volume within the IEG at regularly spaced increments of waveform period for 935 mT magnetic field 7

Figure 5.3, Electrolyte flow velocity as a function of electric field frequency and magnetic field flux density 8

Figure 5.4, Electrolyte flow velocity as a function of electric field frequency and magnetic field flux density where current flow is scaled according to EIS determined conductivity ... 8

List of Tables

Table 3.1, Summary if experimental conditions 5

1 INTRODUCTION

Manufacture of complex micro-scale parts such as biomedical devices and chemical reactors with an excellent surface finish from a wide range of high performance metals has required non-conventional manufacturing processes such as electrochemical machining (ECM). ECM uses anodic dissolution of a workpiece anode in an electrolyte controlled by the shape and proximity of a tool cathode [1]. This process can be assisted using pulsed current between the electrodes, (PECM) [2] and additional reverse polarity pulses can further assist the electrochemical performance of the process by increasing accuracy [3]. Bipolar pulsed electric fields are used in an anodic dissolution electrochemical cell to remove the passivation layer from metals to increase surface quality and efficiency [3, 4, 5, 6].

Since PECM relies on an electrolyte to transfer machining energy to the workpiece there are electrochemical and fluid interactions that play a significant role in process performance [7]. From an electrochemical perspective the literature on ECM discusses pulsed electric fields affect on the electrical double layer (EDL) pseudo-capacitance that causes improvements in conductivity leading to an increase in material removal rate (MRR) performance and surface finish [8, 9]. Magnetic fields are another common way to assist ECM performance [7, 10]. Magnetic fields increase the Lorentz force on the electrolyte in the inter-electrode gap (IEG) increasing electrolyte flow and as a result conductivity to improve ECM performance in terms of accuracy and surface finish [11, 12, 13]. Both PECM and magnetic fields can be combined for a dual-assisted anodic-dissolution processes that combines two different assistances to further increase performance [14, 15, 16]. This type of dual-assisted ECM will generate a complex magnetohydrodynamic (MHD) electrolyte flow in the IEG that will affect performance.

To better control the coupled effects of PECM in a magnetic field to improve ECM performance the combined effects must be studied. Studies in the literature have considered the empirical performance effects of single assisted [2, 12, 13] or dual-assisted ECM involving PECM and magnetic fields [14, 15, 16], which gives little insight into how best to leverage the MHD aspects specifically. Simulations of the MHD effects of ECM electrolyte within either a magnetic field [11, 17] or in a PECM cell [18, 19] has given insight into a similar, but fundamentally different system than the dual-assisted case.

Considering the above state-of-the-literature, this paper introduces a combination of electrochemical impedance spectroscopy (EIS) testing with an MHD simulation representing a magnetically assisted anodic dissolution electrochemical cell. EIS testing gives insight into the effects of the EDL structure on the electrical impedance of the electrochemical cell. The EIS results then drive the electrical current in the MHD simulation to better understand the electrolyte flow within the IEG.

The EIS experimental results show that both the cell voltage frequency and magnet flux density are both significant factors in cell electrical performance. The MHD simulation without the EIS data shows a significant but very different relation of voltage frequency and magnetic field to electrolyte flow velocity. When the computational analysis is combined with the EIS the results suggests operating parameters that differ from either of the two individual results. While these findings indicate an operating regime of higher electrolyte velocities, whether that translates into increased machining performance will require further PECM experiments. Specifically, a design methodology that translates specific machining performance outcomes to input parameters is required to better navigate the complex magnetically assisted PECM design space.

The remainder of the paper is structured as follows. Section 2 outlines the theory related to magnetically assisted PECM. Section 3 presents the details regarding the design of the experimental testbed. Section 4 discusses the computational analysis methodology and Section 5 discusses the findings. Finally, Section 6 outlines the specific conclusions that can be drawn from this study.

2 THEORY

EIS is used to determine the electrical impedance of an electrochemical cell at different sinusoidal frequencies under given cell conditions, in this case a range of magnetic field intensities. The response of the cell to a sinusoidal input should give insights relevant to PECM frequency. An EIS scan measures the complex valued impedance as a function of input voltage and output current according to Ohm's law. Using the reciprocal of impedance, conductance ($|Y|$), Ohm's law is then,

$$I = |Y| \cdot V, \tag{2.1}$$

where I is the total primary current, V is the applied voltage. The magnitude of this current, I, can then be used to drive the applied sinusoidal primary current in the MHD simulation, which determines the current density, $\boldsymbol{J}_{\text{cond}}$.

The MHD simulation requires a solution for the electric and magnetic fields along with the incompressible laminar Navier-Stokes equations. The solution is separated into the time-dependent electric field solution without solving for the induced magnetic field. The low current densities considered in this paper are typical for a comparable PECM cell, but in practice the low current produces a magnetic field much smaller than the minimum field used in this research making the approximation reasonable. The magnetic field is assumed constant over both time and space. The Lorentz force is then a function of current, velocity, and the magnetic field. That volume force is then added to the Navier-Stokes equations to solve for electrolyte velocity.

First the electric field must be solved to find the current density generated by the external potential applied across the electrochemical cell. Charge conservation is enforced using the equation for charge continuity in Eq. 2.2 and is a corollary to the Maxwell equations,

$$\nabla \cdot \mathbf{J}_{\text{cond}} = -\frac{\partial \rho_q}{\partial t}, \tag{2.2}$$

where $\mathbf{J}_{\text{cond}}$ is the current density and ρ_q is the charge density. The Maxwell-Faraday equation yields the general electric potential field $\mathbf{E}$,

$$\mathbf{E} = -\nabla V - \frac{\partial \mathbf{A}}{\partial t}, \tag{2.3}$$

where V is the scalar electric potential, $\mathbf{A}$ is the magnetic vector potential, but to simplify the problem the changing magnetic field is not, which yields,

$$\mathbf{E} = -\nabla V. \tag{2.4}$$

The externally driven current density $\mathbf{J}_{\text{cond}}$ is then,

$$\mathbf{J}_{\text{cond}} = \sigma \mathbf{E} + \frac{\partial \mathbf{D}}{\partial t}, \tag{2.5}$$

where σ is the electrolyte volume conductivity and $\mathbf{D}$ is the electric displacement field.

The continuous form of the Lorentz force is [20],

$$\mathbf{F} = \rho_q \mathbf{E} + \mathbf{J} \times \mathbf{B}, \tag{2.6}$$

where ρ_q is charge density, $\mathbf{J}$ is the total current density, and $\mathbf{B}$ is the constant magnetic field. Solute salt ions will have a hydration shell surrounding them for a net neutral charge resulting in a zero charge density, ρ_q in Eq. 2.6 [21]. This leaves only the cross product of current density with the magnetic field,

$$\mathbf{F} = \mathbf{J} \times \mathbf{B}. \tag{2.7}$$

The current density, $\mathbf{J}$, in the electrolyte results from both electrode conduction in Eq. 2.5 and the induced current, $\mathbf{J}_{\text{ind}}$, caused by the cross product of electrolyte velocity, $\mathbf{u}$, and constant magnetic field, $\mathbf{B}$, according to the Lorentz force in Eq. 2.8,

$$\mathbf{J}_{\text{ind}} = \sigma \mathbf{u} \times \mathbf{B}. \tag{2.8}$$

The total current density is then,

$$\mathbf{J} = \mathbf{J}_{\text{cond}} + \mathbf{J}_{\text{ind}}. \tag{2.9}$$

The constant magnetic field in Eq. 2.6 and Eq. 2.8 is a simplification mentioned earlier that ignores the induced magnetic field generated by the current density, $\mathbf{J}$. Now with a solution for the Lorentz force per unit volume, $\mathbf{F}$, this force can be applied as an external force in the Navier-Stokes equations.

The second step in solving the MHD problem is to determine the electrolyte velocity using the Navier-Stokes equations for laminar incompressible flow,

$$\rho \frac{\partial \mathbf{u}}{\partial t} + \rho(\mathbf{u} \cdot \nabla)\mathbf{u} = \nabla \cdot \left[-p\mathbf{I} + \mu \left(\nabla \mathbf{u} + (\nabla \mathbf{u})^{\mathrm{T}} \right) \right] + \mathbf{F}, \tag{2.10}$$

where ρ is the fluid density, μ is the dynamic viscosity, p is the pressure, and $\mathbf{I}$ is the identity matrix. Equation 2.10 and Eq. 2.8 are coupled in $\mathbf{u}$ requiring a simultaneous solution. Since the flow is incompressible the flow continuity equation simplifies to,

$$\rho \nabla \cdot (\mathbf{u}) = 0. \tag{2.11}$$

Now the solution for the electrolyte velocity, $\mathbf{u}$, and pressure can be evaluated under various conditions. The EIS and simulation each give insight into flow cell function. Using the EIS result to drive the simulation extends the results beyond either individual solutions.

3 Experimental Design

This experimental study used a flat 7075 aluminum alloy workpiece (anode) and a 316 stainless steel tool (cathode). Table 3.1 lists the aluminum alloy composition, which is widely used in

the aerospace industry [22]. The non-ferromagnetic 7075 aluminum and austenitic stainless steel were specifically chosen to leave the constant magnetic field unwarped by ferromagnetic effects [23]. The minimum magnetic field range was the estimated earth's magnetic field shown in Table 3.1. The present study focus on MHD induced flow in an environment representative of PECM. The IEG was maintained at 390 μm in an electrolyte of 20% concentration $NaNO_3$ with no forced flow and a temperature of $21° \pm 1°C$. Sodium nitrate avoids the Cl^- ion corrosion of aluminum associated with NaCl [24]. Both the tool and workpiece surfaces were polished down to a 3,000 grit abrasive. Table 3.1 summarizes experimental conditions for EIS testing. A cut-away of the flow cell used to conduct the EIS testing in shown in Fig. 3.1. The perma-

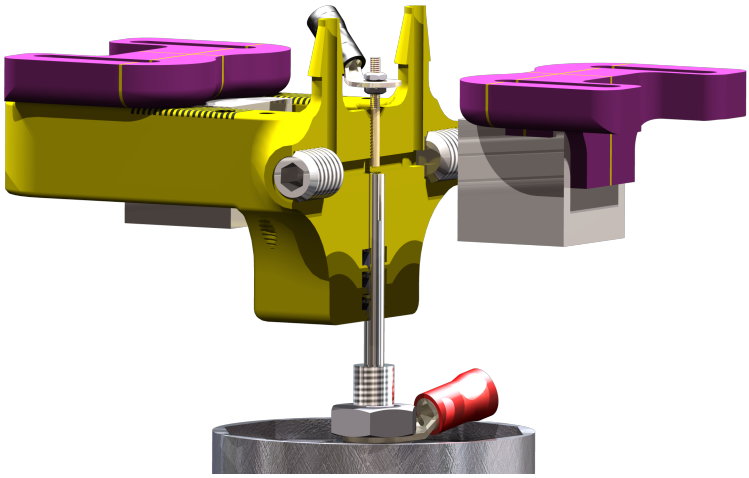

Figure 3.1: Model of Experimental flow Cell

nent magnets shown are one of three sizes used in conjunction with their position to generate various magnetic field flux densities used in the experiments.

A magnetic field map was created using an XY scanning table and an F.W. Bell 5080 Gauss meter with a transverse probe. The field map for the 935 mT field is shown in Fig. 3.2 with the value on the Z-axis derived from the average of measurements within the tool area depicted with the inner cylinder. The outer cylinder depicts the workpiece. Only the magnetic field in the direction from one magnet face to the other was measured as the other directions were orders of magnitude smaller within the IEG.

EIS measurements were taken with a Princeton Applied Research, VeraSTAT3 electrochemical system that measured the impedance one frequency at a time. The spectrum was scanned on a logarithmic scale. The voltages are referenced to a pseudo-reference electrode of 316 stainless steel in contact with the electrolyte [25]. The conductivity in an electrochemical cell is also a function of voltage because the voltage determines whether the cell is operating in the mass transport limited or transpassive state of the EDL [26, 27]. ECM is typically conducted in the transpassive state so the sinusoidal voltage for the EIS scans was on top of a DC voltage to ensure measurements were in the transpassive state.

Table 3.1: Summary of experimental conditions

Workpiece	7075 aluminum alloy cylindrical workpiece Al 89.3%, Cu 1.6%, Mg 25%, Other 1.0%, Zn 5.6%
Tool	1.5 mm diameter 316 stainless steel rod, insulated with acetal resin annulus
Process	– $NaNO_3$ Mass Concentration: 20% – Temperature: 20°-22°C – Inter-electrode gap : 390 μm
Sine Input-$\boldsymbol{V}$	– Voltage: ±0.10V – Frequency: 0.25 Hz-250 kHz – Offset Voltage: 1.15V-1.25V
Magnetic Field-**B**	– Flux Density 0.055 mT-935 mT
Output-$\lvert Y \rvert$	– Conductance: (mS)

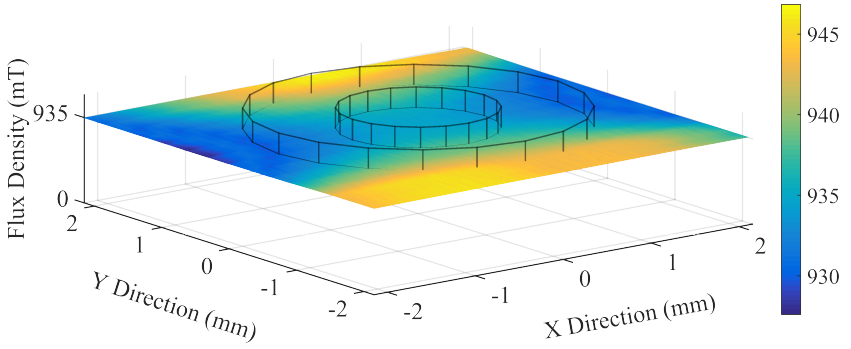

Figure 3.2: Map of magnetic field flux density within the IEG with the inner cylinder representing the tool IEG and the outer cylinder the workpiece

4 Numerical Model

The simulation emulates the basic geometry used for the EIS experiments with the same tool and workpiece diameter along with the same IEG and flow channel dimensions. Additionally the electrolyte properties of conductivity, σ, and density, ρ were matched. The computational analysis were conducted in COMSOL 5.2® using the AC/DC module to solve Maxwell's equations and the Multiphisics® module to solve the laminar Navier-Stokes equations. The diagram in Fig. 4.1 shows the geometry for the simulation with the instantaneous vectors representing the magnetic field shown in "red", the general electric field shown in "yellow", the general resulting Lorentz force in "black", and the general electrolyte flow shown in "blue".

The outer cylinder shown in Fig. 4.1 that is defined by the workpiece outer diameter is the boundary of the IEG. The average velocity magnitude of the electrolyte within the IEG is used as

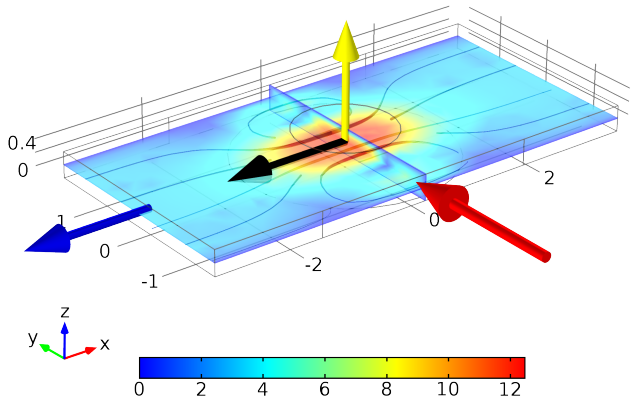

Figure 4.1: Simulation showing vectors for magnetic field, electric field, Lorentz force, and resulting electrolyte flow

the performance metric for each time step. The maximum of this velocity is taken over the three frequency periods for each simulation run and this velocity is the scalar performance metric used to compare simulations at each frequency and magnetic field. The sinusoidal current input for the MHD simulation has a constant magnitude, while the combined MHD simulation current calculated from the product of a constant voltage and conductivity.

5 Results and Discussion

The solution for the EIS testing indicates the relationship of the electrolyte conductivity, $|Y|$, as a function of magnetic flux density and the applied voltage frequency, which is of interest on its own as an indicator of electrochemical response. Likewise, the MHD solution based on a constant magnitude sine wave gives a more general indication of the flow effects in a given environment without regard to a specific electrochemistry. By combining the two solutions the result more closely approximates the specific environment allowing a more directed study of magnetically assisted PECM.

5.1 EIS Conductivity

In Fig. 5.1 the surface that represents the conductivity, $|Y|$ is on a logarithmic scale in both frequency and magnetic field. The conductivity surface was produced by averaging six tests at three offset voltages ranging from 1.15V to 1.25V for a given magnetic flux density. This result shows that higher frequency is directly proportional to conductivity, which is consistent with other studies [26, 19]. The relation between conductivity and the magnetic field looks to have a maximum in the middle of the range around 46 mT, also similar to another study [10].

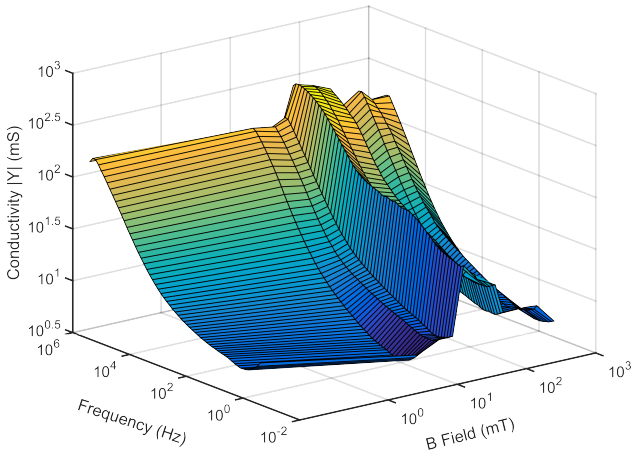

Figure 5.1: EIS conductivity as a function of frequency and magnetic field flux density

5.2 MHD Simulation

The simulation shown in Fig. 4.1 was solved in the time domain over three sinusoidal periods at the same frequencies and magnetic fields that the EIS scans were run. The bounding of the MHD simulation to three periods is necessary to maintain a consistent computational load between frequencies at this small time scale [28, 29]. Figure 5.2 shows all the data used for the 935 mT simulation at a constant sinusoidal voltage input. The simulation in Fig. 5.2 runs for

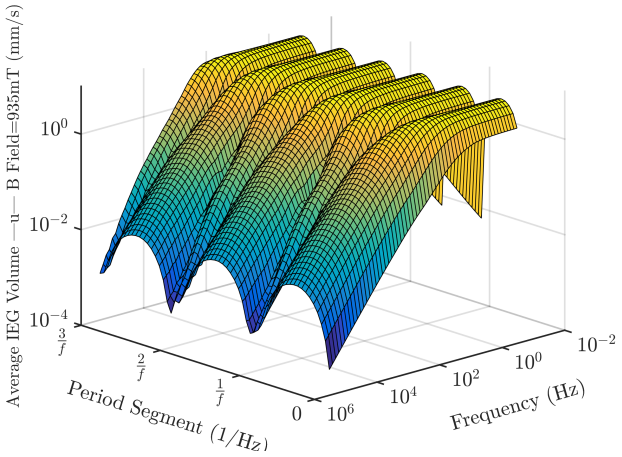

Figure 5.2: Electrolyte velocity magnitude averaged over the volume within the IEG at regularly spaced increments of waveform period for a 935 mT magnetic field

three periods, the velocity magnitude at high frequencies shows three maximums where the electrolyte is accelerated during the positive portion of sinusoid and is then decelerated during the negative portion for a pulsing effect. As the voltage input increases in frequency the electrolyte flow begins to reverse direction more until the forward and reverse velocity magnitudes are equal from about 10 Hz and below.

The simulation data from Fig. 5.2 is combined with the data at the other magnetic field intensities to form the surface plot in Fig. 5.3. The surface in Fig. 5.3 suggests operating at the highest

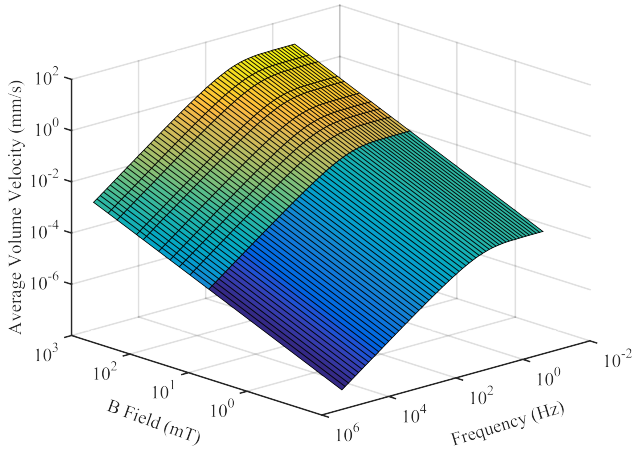

Figure 5.3: Electrolyte flow velocity as a function of electric field frequency and magnetic field flux density

magnetic field and at any frequency below roughly 10 Hz to maximize electrolyte velocity.

5.3 EIS Driven MHD Simulation

Data collected at the same levels in the EIS can now be introduced into a new MHD simulation to rerun the computational analysis. The surface plot for the combined simulation in Fig. 5.4 is similar to Fig. 5.3. The most prominent difference is now there is an apparent maximum for each magnetic field intensity around 10 Hz. The absolute maximum for velocity is still at the maximum magnetic field of 935 mT.

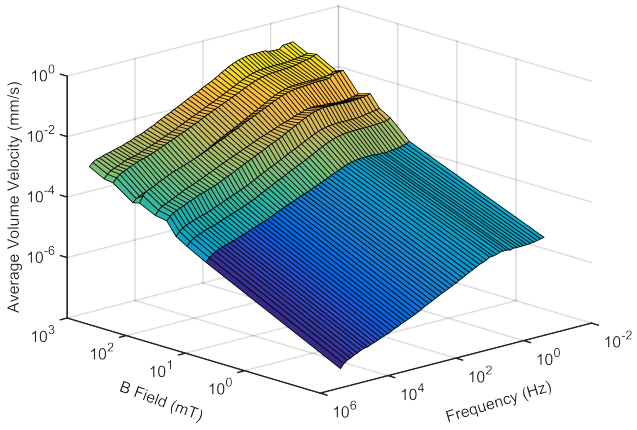

Figure 5.4: Electrolyte flow velocity as a function of electric field frequency and magnetic field flux density where current flow is scaled according to the EIS determined conductivity

6 Conclusion

Both EIS testing and MHD simulations show that the electrolyte flow velocity within the IEG is highly dependent on both the electric field frequency and magnetic field flux density. The EIS results suggests operating at a higher electric field frequency to maximize cell conductivity. The purely MHD computational result suggests minimizing the electric field frequency and maximizing the magnetic field to maximize electrolyte velocity. Combining the EIS results with the MHD computational analysis suggests an optimum electric field frequency to maximize the electrolyte flow velocity.

The results of this computational analysis will allow a more focused experimental validation of the effects of electric field frequency and magnetic field flux density on PECM machining performance. Using machining metrics like material removal rate, surface finish and accuracy will give insight into where in the operating space the various input parameters dominate each machining response. It is possible that different operating points will differ in performance between each metric where increasing one may diminish another.

Acknowledgments

This research is funded by the U.S. Army - Armament Research, Development and Engineering Center (ARDEC), Internal Lab Independent Research (ILIR) Grant; and the U.S Army-ARDEC, Science Fellowship Grant.

References

[1] F Pitschke. General applications of electrochemical machining. Technical Report 620205, SAE Technical Paper, Troy, MI, USA, Jan. 1962.

[2] M. Datta and D. Landolt. Electrochemical machining under pulsed current conditions. *Electrochimica Acta*, 26(7):899–907, Jul. 1981.

[3] T. Masuzawa and M. Kimura. Electrochemical surface finishing of tungsten carbide alloy. *CIRP Annals*, 40(1):199–202, Jan. 1991.

[4] A Zaytsev, I Agafonov, N Gimaev, R Moukhoutdinov, and A Belogorsky. Precise pulse electrochemical machining by bipolar current: Aspects of effective technological application. *Journal of Materials Processing Technology*, 149(1):419–425, 2004.

[5] Ronnie Mathew and Murali M. Sundaram. Modeling and fabrication of micro tools by pulsed electrochemical machining. *Journal of Materials Processing Technology*, 212(7):1567–1572, Jul. 2012.

[6] Wataru Natsu and Daiki Kurahata. Observation of workpiece surface in ecm process of wc alloy micro-pin with bipolar pulses. *International Journal of Electrical Machining*, 21(0):31–38, Feb. 2016.

[7] Piyushkumar B. Tailor, Amit Agrawal, and Suhas S. Joshi. Evolution of electrochemical finishing processes through cross innovations and modeling. *International Journal of Machine Tools and Manufacture*, 66:15–36, Mar. 2013.

[8] M. Inman, T. Hall, E.J. Taylor, C.E. Reece, and O. Trofimova. Niobium electropolishing in an aqueous, non-viscous hf-free electrolyte: A new polishing mechanism. In *Proceedings of SRF2011, Chicago, IL*, pages 377 – 381, Jun. 2011.

[9] Jeong Woo Park and Deug Woo Lee. Pulse electrochemical polishing for microrecesses based on a coulostatic analysis. *The International Journal of Advanced Manufacturing Technology*, 40(7-8):742–748, Feb. 2009.

[10] J.C. Fang, Z.J. Jin, W.J. Xu, and Y.Y. Shi. Magnetic electrochemical finishing machining. *Journal of Materials Processing Technology*, 129(1-3):283–287, Oct. 2002.

[11] Oleg Lioubashevski, Eugenii Katz, and Itamar Willner. Magnetic field effects on electrochemical processes: A theoretical hydrodynamic model. *The Journal of Physical Chemistry B*, 108(18):5778–5784, May. 2004.

[12] Zhijian Fan, Tiancheng Wang, and Ling Zhong. The mechanism of improving machining accuracy of ecm by magnetic field. *Journal of Materials Processing Technology*, 149(1-3):409–413, Jun. 2004.

[13] L. Tang and W.M. Gan. Experiment and simulation study on concentrated magnetic field-assisted ECM S–03 special stainless steel complex cavity. *The International Journal of Advanced Manufacturing Technology*, 72(5-8):685–692, May. 2014.

[14] P. S. Pa. Design of a magnetic-assistance superfinish module for freeform machining. *Journal of Vacuum Science & Technology B Microelectronics and Nanometer Structures*, 27(3):1221–1225, May. 2009.

[15] P.S. Pa. Mechanism design of magnetic-assistance in surface finishing of end-turning. *Journal of Advanced Mechanical Design Systems and Manufacturing*, 2(4):587–596, Jul. 2008.

[16] Liang Yin, Wei-min Zhang, Yong Yan, Qing-song Tu, and Zhi-jing Zhang. Study of electrochemical finishing with magnetic field and high-frequency group pulse. In *2010 International Conference on Digital Manufacturing & Automation*, volume 2, pages 440–443, Dec. 2010.

[17] Li Long, MA Baoji, Wang Ruifeng, and Du Lingqi. The coupled effect of magnetic field, electric field, and electrolyte motion on the material removal amount in electrochemical machining. *The International Journal of Advanced Manufacturing Technology*, 91(9–12):2995–3006, Aug. 2017.

[18] Olivier Weber, Andreas Rebschläger, Philipp Steuer, and Dirk Bähre. Modeling of the material/electrolyte interface and the electrical current generated during the pulse electrochemical machining of grey cast iron. In *Proceedings of the European COMSOL Conference*, pages 1–6, Oct. 2013.

[19] Olivier Weber, Harald Natter, and Dirk Bähre. Pulse electrochemical machining of cast iron: A Layer-based approach for modeling the steady-state dissolution current. *Journal of Solid State Electrochemistry*, 19(5):1265–1276, May. 2015.

[20] David J Griffiths. *Introduction to Electrodynamics, 3rd ed.* Prentice-Hall, Upper Saddle River, NJ, USA, 1999.

[21] Yizhak Marcus. *Ions in Water and Biophysical Implications: From Chaos to Cosmos.* Springer Science & Business Media, Dordrecht, Netherlands, 2012.

[22] Richard Shepherd Shevell. *Fundamentals of Flight.* Prentice-Hall, Englewood Cliffs, NJ, USA, 1983.

[23] A.A. Tavassoli. Assessment of austenitic stainless steels. *Fusion Engineering and Design*, 29:371–390, Mar. 1995.

[24] R.E. Stoltz and R.M. Pelloux. Inhibition of corrosion fatigue in 7075 aluminum alloys. *Corrosion*, 29(1):13–17, Jan. 1973.

[25] György Inzelt, Andrzej Lewenstam, and Fritz Scholz. *Handbook of Reference Electrodes.* Springer, Heidelberg, Germany, 2013.

[26] Weidong Liu, Sansan Ao, Yang Li, Zuming Liu, Hui Zhang, Sunusi Marwana Manladan, Zhen Luo, and Zhiping Wang. Effect of anodic behavior on electrochemical machining of tb6 titanium alloy. *Electrochimica Acta*, 233:190–200, Apr. 2017.

[27] M Datta and D Landolt. High rate transpassive dissolution of nickel with pulsating current. *Electrochimica Acta*, 27(3):385–390, 1982.

[28] Curtis Bradley. *Electrochemical Machining Assisted Using Pulsed Electric Fields, Ultrasonic Motion, and Magnetic Fields.* PhD thesis, Rensselaer Polytechnic Institute, 2018.

[29] Ingo Schaarschmidt, Matthias Hackert-Oschätzchen, Gunnar Meichsner, Mike Zinecker, and Andreas Schubert. Implementation of the machine tool-specific current and voltage control characteristics in multiphysics simulation of electrochemical precision machining. *Procedia CIRP*, 82:237–242, 2019.